Power Electronic Devices and Components 4 (2023) 100034

Contents lists available at ScienceDirect

Power Electronic Devices and Components

journal homepage: www.journals.elsevier.com/power-electronic-devices-and-components

Invited Paper

Lifetime modeling of solder joints based on accelerated mechanical testing and Finite Element Analysis

M. Lederer *, A. Betzwar Kotas, G. Khatibi

Christian Doppler Laboratory for Lifetime and Reliability of Interfaces in Complex, Multi-Material Electronics, Institute for Chemical Technologies and Analytics, TU Wien, Getreidemarkt 9, 1060 Vienna, Austria

ARTICLE INFO

Keywords:
Solder fatigue
Lifetime model
Coffin-Manson model
Goodman relation
Damage accumulation

ABSTRACT

Solder fatigue is among the predominant failure modes observed in power electronic modules. Under service conditions power electronic parts are exposed to repeated temperature swings originating from resistance heating. In consequence of a mismatch of the coefficients of thermal expansion, thermomechanical stresses are generated at material interconnects. Nevertheless, lifetimes of up to 30 years are requested for high reliability applications. Therefore, there is a demand for accelerated testing methods. However, due to strain rate dependence of inelastic deformations theoretical lifetime modeling is necessary to compare the results of accelerated test methods with usual service conditions. The present study reports on a mechanical testing method operating at the ultrasonic frequency of 20 kHz. During testing samples are exposed to repeated bending deformations until the solder joint finally breaks. The number of cycles to crack initiation is determined for different temperatures ranging from room temperature to 175 °C. Thereafter, an FEM computer simulation of the fatigue experiment is performed, where the visco-plastic Anand model serves as material model of the solder. The time to crack initiation in the solder is evaluated with a model of damage accumulation, which combines the Coffin-Manson model with a multiaxial version of the Goodman relation. It is demonstrated that this model can be applied to the solder alloys PbSnAg, Sn3.5Ag and SnSbAg.

Introduction

Under service conditions power electronic devices are exposed to repeated temperature swings caused by resistive heating. Owing to different coefficients of thermal expansion of the constituent materials considerable thermomechanical stresses are observed at material interconnects. Nevertheless, lifetimes of up to 30 years are requested for high reliability applications as e. g. railway traction. Such a high reliability level can only be achieved by combination of advanced engineering design and comprehensive lifetime testing.

Lifetime models designed for specific applications are often based on a weakest link approach. When several competing failure modes are observed, then the various reliability issues are taken into account with respect to their statistical probabilities, respectively. In the case of insulated gate bipolar transistor (IGBT) modules, the predominant failure modes observed under operation condition are wire-bond failure (Sathik et al., 2015; Czerny et al., 2012; Schmidt & Scheuermann, 2012) and solder fatigue (Herrmann et al., 2007; Dudek et al., 2019). The present study is devoted to the investigation of solder fatigue caused by thermal and mechanical loads.

The most common standard methods for testing the fatigue life of power modules are thermal cycling (Sathik et al., 2015), power cycling (Sathik et al., 2015; Schmidt & Scheuermann, 2012; Herrmann et al., 2007) and vibration tests (Yu et al., 2011; Libot et al., 2016). In the majority of cases, reliability tests are carried out under steady state conditions consecutively performed at different load levels. The regime of low cycle solder fatigue is characterized by accumulation of plastic strain. The material fatigue in this regime is well described by the Coffin (1971)-Manson (Manson & Hirshberg, 1964) model, which is a power law relating the plastic strain increase per loading cycle to the number of loading cycles to failure. On the other hand, high cycle fatigue at load levels well below the yield stress is better described by the Basquin equation (Basquin, 1910), or by more recent reformulations of this approach describing the fatigue life as function of the applied stress level (Thambi et al., 2016).

Furthermore, there are several lifetime models considering the influence of both, elastic and plastic deformations. A quite simple, but very successful model for solder fatigue ranging from low to high cycles is the

* Corresponding author.
E-mail address: martin.lederer@tuwien.ac.at (M. Lederer).

https://doi.org/10.1016/j.pedc.2023.100034
Received 14 September 2022; Received in revised form 13 December 2022; Accepted 23 January 2023
Available online 25 January 2023

Engelmaier model relating the fatigue life to the total shear strain Engelmaier (1983). A reformulated version of this model was proposed by Salmela et al. (2008), who introduced a correction term to account for the different stress levels a solder material experiences. Another possibility of considering elastic and plastic deformations is the combined Coffin-Manson-Basquin equation (Morrow, 1964), where four material parameters are used to estimate the lifespan of samples exposed to cyclic deformations. An extended version of this approach was proposed by Wang et al. (2019), who brought a Taylor expansion to the third order to describe the temperature dependence of the material parameters.

Another important aspect consists in the effect of nonzero mean stress resulting in reduced fatigue life. For states of uniaxial stress, the correlated fatigue life can be evaluated with standard methods developed by Goodman (1899), Gerber and Soderberg. A multiaxial treatment of this method was proposed by Susmel et al. (2005), who introduced the critical plane approach. In the present study, a modified version of the multiaxial mean stress approach will be proposed, where the contributions to fatigue arising from different components of deviatoric stress are evaluated by analogy to the von Mises stress equivalent.

Under service conditions, load levels are changing during the lifespan of power electronic devices. The damage originating from different stress amplitudes can be evaluated with use of the rainflow counting method (Marsh et al., 2016; Mainka et al., 2011). Finally, the contributions to material fatigue are usually added according to Miner's rule of linear damage accumulation (Miner, 1945).

In the present investigation, two different mechanisms of solder fatigue are considered. Firstly, the accumulation of damage arising from plastic strain is calculated by analogy to the Coffin-Manson model. Secondly, an effect of non-zero multiaxial mean stress is suggested, where the temperature dependence of this effect is to some extent attributed to the temperature dependence of the solders Young's modulus. This effect is related to the elastic strain amplitude. The damage arising from either contribution is added according to Miner's rule of linear damage accumulation. This model of damage accumulation is combined with the visco-plastic Anand model, which serves as material model for the solder. Thus, one obtains a lifetime model of wide applicability, which can be used at various temperatures and strain rates. According to the hypothesis proposed in this article, the results of fatigue experiments derived from accelerated mechanical tests performed at different temperatures can now be applied to lifetime predictions of power electronic devices under service conditions.

Finally, the coefficients of the lifetime model are obtained from numerical fits to fatigue experiments. For this purpose, accelerated mechanical fatigue tests were performed in three and four point bending at temperatures between room temperature and 175 °C. Three different solder alloys were selected for this investigation: PbSnAg has extensively been analysed in recent years, and therefore sufficient literature data are available, which can now be used as benchmark for model validation. The second solder material of this study is the lead-free alloy Sn3.5Ag, which is nowadays widely used in industry. The third solder alloy, SnSbAg, has gained increasing interest in recent years, because of its excellent mechanical properties resulting in high strength and durability.

The time dependent loading conditions were simulated by fully transient Finite Element Analyses in order to obtain time history data of stresses and strains at the critical sites, where crack initiation occurs. The FEM simulations were conducted with ANSYS 2020.

Experimental

Sample design, sample preparation and experimental setup

There are two main types of large area solder joints, which are used in power electronic devices: The first type connects a silicon chip to a direct bonded copper (DBC) substrate, while the second type connects the DBC structure to a baseplate. The devices under test investigated here are model solder joints, which have the purpose to mimic the solder interconnects used in power electronics. In this series of experiments, the solder joints had a thickness of 100 μm. In order to perform high cycle fatigue tests within reasonable time, an accelerated mechanical test method operating at an ultrasonic frequency of 20 kHz was employed. The samples were designed to fulfill resonance conditions at the testing frequency. Eigenmodes of the samples related to this resonant frequency are depicted in Figs. 1, and 2. These eigenmodes can be excited by setups of three- or four-point bending, respectively.

The bending mode used in the fatigue test is selected in accordance with the sample geometry. For a given mode shape, the requirement that a sample must be in resonance at 20 kHz dictates the ratio of sample length to substrate thickness. During deformation, the largest strain should occur in the solder material. Furthermore, a preload is needed to ensure that ultrasonic horn and supporting jigs are in permanent contact with the sample. It must be avoided that the ultrasonic horn takes off from the sample periodically, because hammering against the sample could lead to a different failure mode. Moreover, the contact points where jigs and ultrasonic horn touch the sample should be sufficiently far away from the solder joint and the silicon chip in order to avoid friction at the solder material or damage of the chip.

The DBC structure of the sample depicted in Fig. 1 consisted of a copper - alumina - copper sandwich structure with two copper layers of 8 mm x 8 mm x 0.3 mm and an alumina layer of 9 mm x 9 mm x 0.32 mm in between. The whole DBC structure was soldered onto a copper plate of 25.04 mm x 10 mm x 3 mm. This sample was used for the setup of three-point bending.

On the other hand, the DBC substrate of the sample shown in Fig. 2 had a length of 43.2 mm and a width of 9.7 mm. Further, the DBC substrate consisted of two 0.3 mm thick copper layers with a 0.63 mm thick alumina layer in between. A silicon chip with dimensions of 11 mm x 9.7 mm x 0.42 mm was soldered onto the DBC substrate. This sample was used in combination with the setup of four-point bending.

The complete setup of the fatigue tests is shown in Fig. 3. An ultrasonic generator is connected to a piezoelectric transducer, which induces periodic vibrations in an acoustic horn. The maximal displacement amplitude is observed at the end of the horn. Further, the tip at the end of the horn is in contact with the device under test. At the opposite side, the sample is supported by rigid jigs. In consequence, the device under test is subjected to periodic bending vibrations. Samples shown in Figs. 1 and 2 were oriented with the substrate at the upside so that the soldered part fell down at the end of life. The magnitude of the periodic displacements observed at the sample center during vibration was measured with a Laser Doppler Vibrometer (LDV). It has already been mentioned that static preload was applied to the specimens in order to keep the vibrating sample in permanent contact with the supporting jigs. In the case of the three-point bending setup, the preload was typically 70 N, while a preload of 65 N was used in combination with the four-point bending setup.

In view of the enforced periodical vibrations, stresses are generated in the device under test. Owing to its low melting point, the solder alloy is the weakest material. When the periodic deformations are large enough, one observes crack initiation at the location, where the solder joint experiences the largest strain. However, crack initiation is delayed by the ductility of the solder material. The time until first crack initiation is measured by acoustic emission using an optical microphone of the company Xarion. Thereby, the optical microphone utilizes Fast Fourier Transformation (FFT) to filter out the acoustic signal of cracking from the surrounding noise of the ultrasonic setup. The noise of the setup typically occurs at the 20 kHz resonance frequency and at its correlated higher harmonics, while acoustic emission of cracking is found at a different frequency. When the signal of cracking is detected, then the fatigue experiment is interrupted and the existence of a crack is validated by optical inspection with Scanning Electron Microscopy. In the frame of the present study, a sample is considered to contain a first

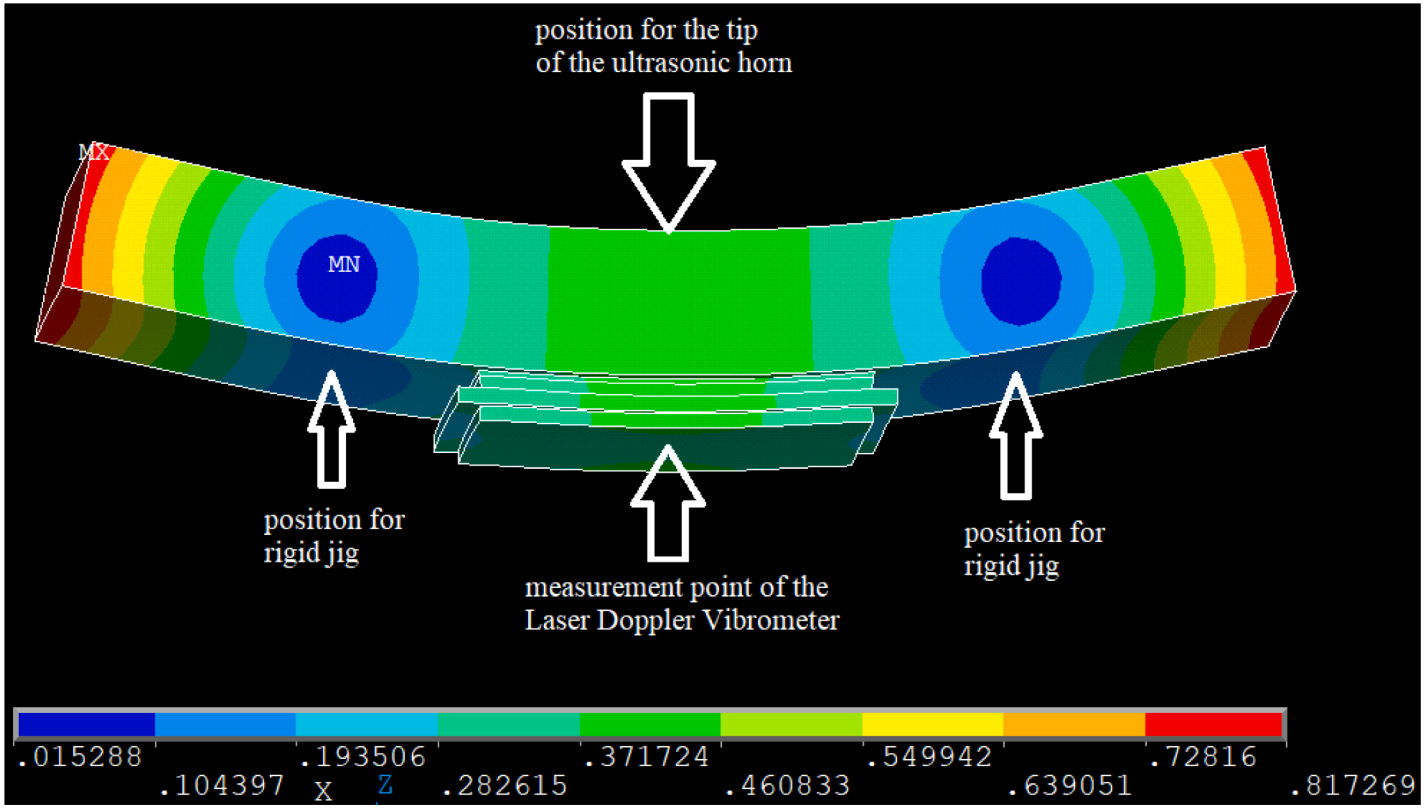

Fig. 1. FEM modal analysis of an unconstrained sample. A plot of the displacement vector sum is shown. This eigenmode can be excited by three-point bending. The positions, where boundary conditions are applied in the experiment, are indicated.

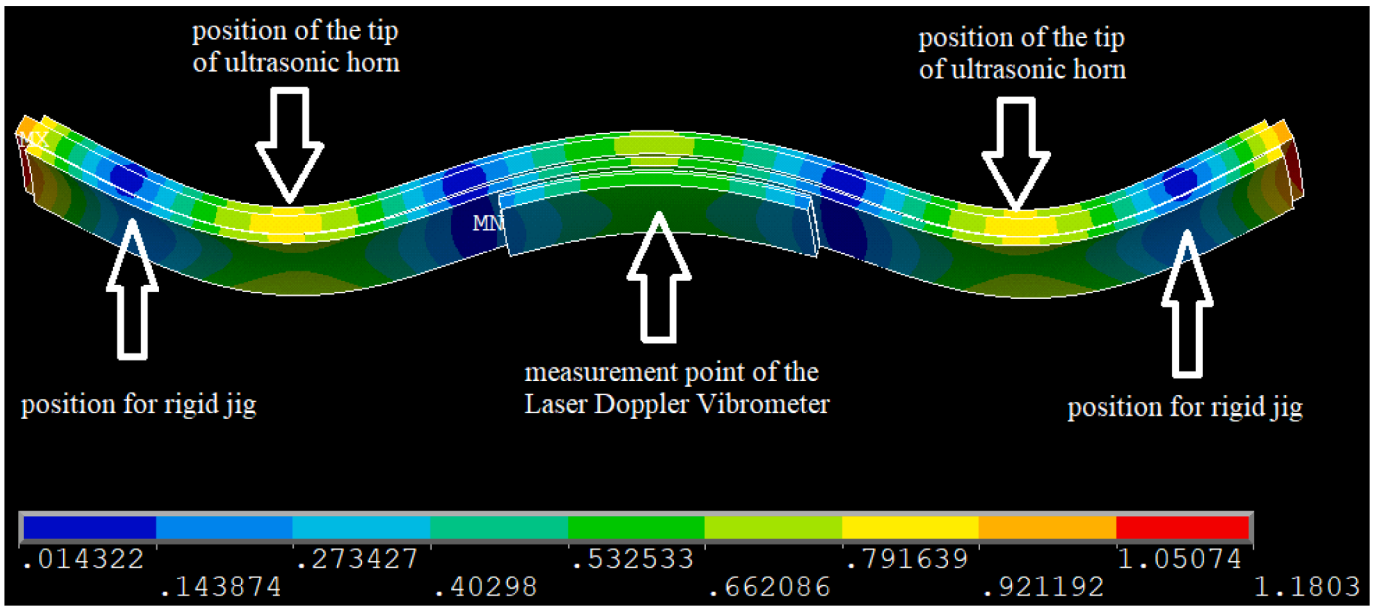

Fig. 2. FEM modal analysis of an unconstrained sample. This mode shape can be excited by four-point bending. The positions, where boundary conditions will be applied in the experiment are shown.

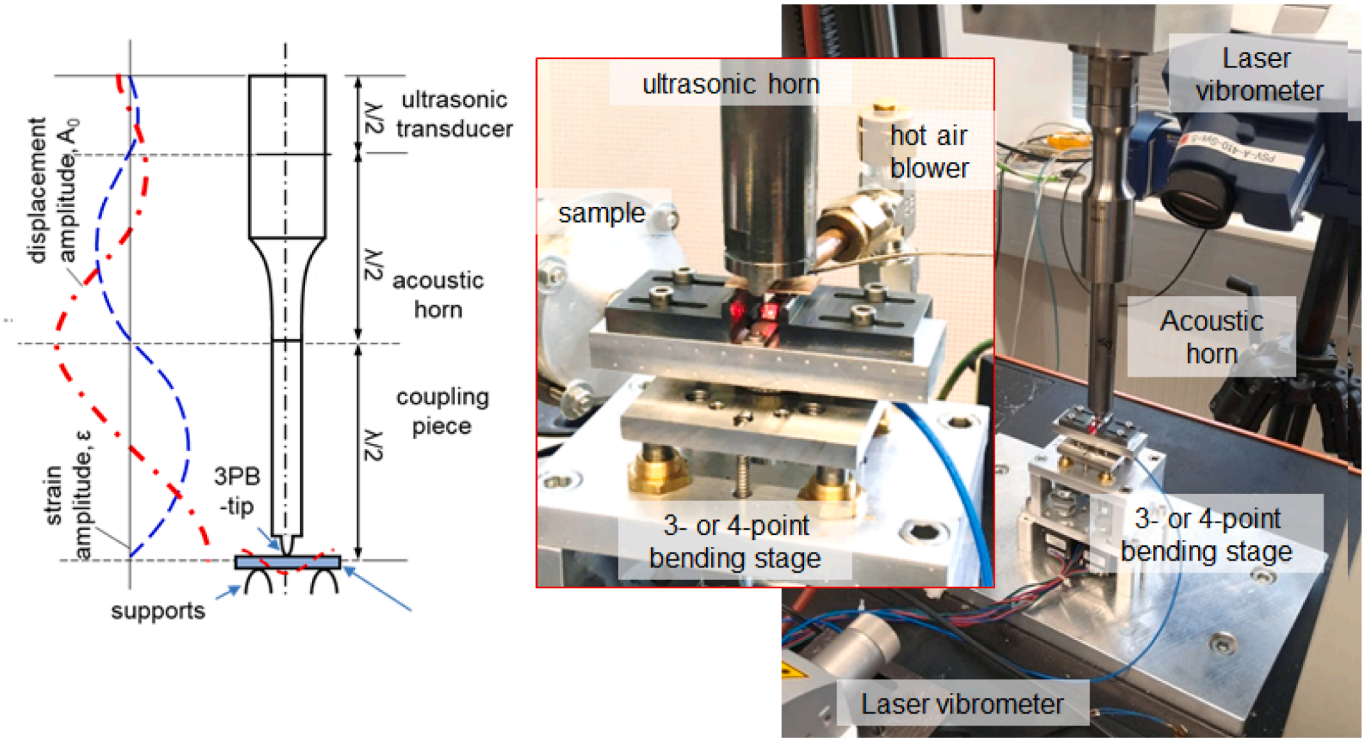

Fig. 3. Left: The experimental setup of the ultrasonic fatigue experiment, schematically. Middle and right: Photos of the complete experimental setup.

crack, when the visible crack length is at least 100 μm.

For selected specimens, the path of crack propagation was documented by intermittent tracing of the crack front observed by optical inspection. The number of cycles until end of life was determined for the moment, when the cracked part of the sample fell off from the substrate.

Fractography

The existence of a first crack in a sample was validated by optical inspection. For this purpose, fatigue experiments were interrupted and the visible crack length was measured with use of SEM micrographs. Crack initiation occurred at the periphery of the solder joints near to the position, where maxima of accumulated plastic strain were found in FEM simulations. During optical inspection, samples were rotated inside the Scanning Electron Microscope to see the soldered joint from every side. However, cutting of the sample was avoided so that the fatigue experiment could be continued until finally the soldered part detached from the substrate. In the present study, samples were considered as cracked, when the crack length exceeded 100 μm. Examples for specimens containing a first crack are depicted in Fig. 4.

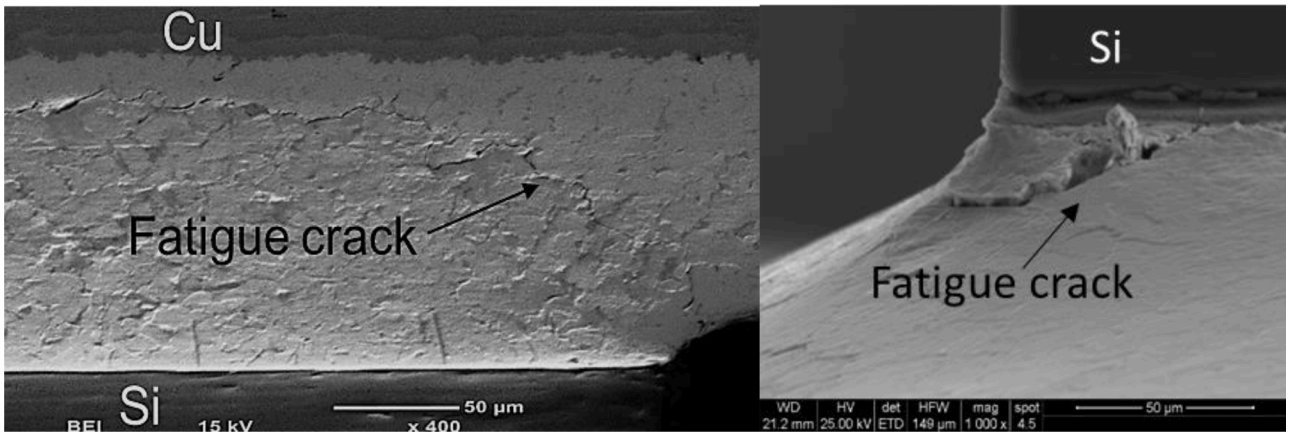

Fig. 4. Left: Crack at the periphery of a PbSnAg solder joint. Right: Crack at the corner of an SnSbAg solder joint.

Experimental results

Experimental results for number of loading cycles to failure at different load levels were collected for the solder alloys PbSnAg, Sn3.5Ag and SnSbAg. Experiments in the three-point bending mode were performed at temperatures of 25 °C, 80 °C, and 125 °C, while four-point bending was applied at 175 °C. The displacement amplitudes observed at the middle of a sample were measured with a Laser Doppler Vibrometer. This information about periodical displacements is necessary for calibration of the Finite Element simulations, which are used to determine the stress distribution in the vibrating specimen.

The fatigue experiments comprise measurements of time to initiation of a first crack and tests until end of life, when the entire chip lifts off from the substrate. For the solder joint geometries investigated here, the time to first crack initiation is approximately 25% of the entire lifetime. A plot of time to first crack initiation versus displacement amplitude of PbSnAg samples tested at 175 °C is shown in Fig. 5. Averaged experimental values for time until first crack initiation of PbSnAb, Sn3.5Ag and SnSbAg solders can be found in Tables 1–3.

A comparison between fatigue lives of all three solder alloys tested under identical conditions can be found in Figs. 6 and 7. Obviously, the lead free solder alloys showed superior lifetime. Therefore, Sn3.5Ag and SnSbAg were also tested at larger displacement amplitudes as depicted in Fig. 8.

FEM simulations

In order to obtain further insight into the mechanism of crack initiation, FEM computer simulations were carried out with ANSYS 2020. It was found that the fatigue life of solders is a result of complex material

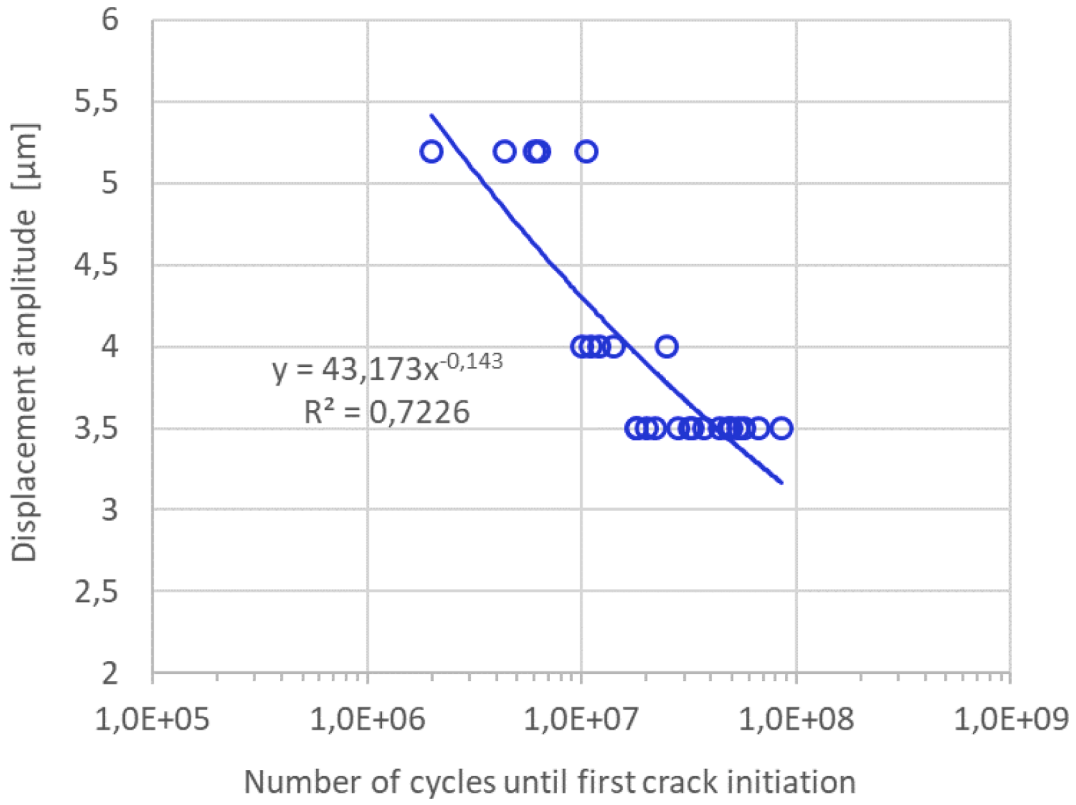

Fig. 5. Number of loading cycles until first crack initiation versus displacement amplitude for samples soldered with PbSnAg and tested in four point bending mode at 175 °C.

Table 1
Statistical averages for number of loading cycles until first crack initiation for samples soldered with PbSnAg.

Temperature	Bending Mode	Displacement Amplitude	Number of tested samples	Number N_f of cycles to first crack
25 °C	3-point bending	5.2 µm	10	$1.5{\cdot}10^6$
25 °C	3-point bending	6 µm	10	$7.6{\cdot}10^5$
80 °C	3-point bending	4 µm	5	$1.1{\cdot}10^6$
80 °C	3-point bending	6 µm	5	$7.7{\cdot}10^4$
125 °C	3-point bending	5.2 µm	5	$1.2{\cdot}10^4$
175 °C	4-point bending	3.5 µm	10	$2.8{\cdot}10^7$
175 °C	4-point bending	4 µm	5	$1.4{\cdot}10^7$
175 °C	4-point bending	5.2 µm	10	$5.7{\cdot}10^6$

Table 2
Statistical averages for number of loading cycles until first crack initiation for samples soldered with Sn3.5Ag.

Temperature	Bending Mode	Displacement Amplitude	Number of tested samples	Number N_f of cycles to first crack
125 °C	3-point bending	5.2 µm	5	$2.1{\cdot}10^5$
125 °C	3-point bending	6 µm	5	$1.2{\cdot}10^5$
125 °C	3-point bending	7 µm	5	$7.5{\cdot}10^4$
175 °C	4-point bending	5.2 µm	10	$2.6{\cdot}10^7$

Table 3
Statistical averages for number of loading cycles until first crack initiation for samples soldered with SnSbAg.

Temperature	Bending Mode	Displacement Amplitude	Number of tested samples	Number N_f of cycles to first crack
80 °C	3-point bending	6 µm	8	$1.1{\cdot}10^6$
125 °C	3-point bending	5.2 µm	5	$7.9{\cdot}10^5$
125 °C	3-point bending	6 µm	5	$3.3{\cdot}10^5$
125 °C	3-point bending	7 µm	5	$1.3{\cdot}10^5$
175 °C	4-point bending	5.2 µm	10	$5.4{\cdot}10^7$

behavior depending on accumulated plastic strain, alternating stress and mean stress occurring at the critical sites of the samples.

Analysis type

The loading conditions at the different temperatures were simulated in fully transient analyses, where every period of oscillation was divided into 25-time steps. The simulation of the experiments started with heating from room temperature and mechanical preloading of the sample. Thereupon, periodic forces are transferred to the contact areas leading to increasing displacement amplitudes during the first oscillations. Note that the operating frequency of the test method is very close to the resonant frequency, and therefore approximately 40 periods were needed until steady state oscillations were derived. An example for the time history of displacement at the sample center is shown in Fig. 9. The periodical loads assumed in the simulation were adjusted until the simulated displacement amplitudes were in accordance with experimental values. The displacement offset, which can be seen in Fig. 9, is due to the preload applied to the sample.

Material models

Material models for the devices were chosen in agreement with literature data (Wilde et al., 2000; Chen et al., 2004; Cheng et al., 2000; Kobayashi et al., 2018; El-Daly et al., 2011; Murty et al., 1997). The solder materials were simulated according to the visco-plastic Anand model (Anand, 1985) using the parameters summarized in Table 4.

Copper was simulated in isotropic elastic approximation combined with Rayleigh material damping using the coefficients $\alpha = 4{\cdot}10^3$ $[sec]$ and $\beta = 4{\cdot}10^{-11}$ $[sec^{-1}]$. Silicon and the ceramic Al_2O_3 were simulated in elastic approximation assuming negligible material damping. The material parameters for the elastic properties, for thermal expansion and for density are summarized in Table 5.

Geometry and mesh

Only the essential parts of the experimental setup were modelled in detail. The ultrasonic horn and the supporting jigs at the bottom side were modelled as boundary conditions. Preload and periodical forces were supplied to the contact area, where the tip of the ultrasonic horn hits the sample as sketched in Figs. 1 and 2, respectively. Due to symmetry conditions, it was possible to reduce the model to a quarter of the complete sample. Attention was paid to realistic modeling of solder joints. Fig. 10 shows the theoretical model of the solder geometry in comparison with an SEM micrograph of a test sample. The mesh was generated with element type Solid 186 of ANSYS classic using a constant element size of 100 µm in the solder material. The solder geometry was the same for all three solder materials, and the constant element size within the solder had the purpose to reduce the mesh size dependence. In consequence, the highest stress concentrations were always found at typical sites of the sample either at a corner or at the edge of the solder geometry.

Simulation results

The evolution of stresses and strains observed in the FEM simulation is used as input to the lifetime model. Fracture will occur at a critical site, where the accumulated damage reaches a maximum. Therefore, a damage variable shall be defined, which depends on stresses and strains.

Fig. 11 shows a plot of accumulated plastic strain in a sample after 40 loading cycles. The evolution of the stress component σ_{11} at this point during the first 40 loading cycles is depicted in Fig. 12. For evaluation of the damage variable defined in the next section, it will be necessary to collect the data of all stress components in addition to accumulated plastic strain.

Lifetime model

The lifetime model proposed here estimates the time to crack initiation in the solder joint. The idea behind this approach is to develop an advanced fatigue model by merging principles included in various standard models. In particular, we combine the Coffin-Manson-Basquin model with a multiaxial treatment of the Goodman relation describing the effect of non-zero mean stress. Thereby, the contributions to material fatigue arising from the different failure mechanisms are added according to Miner's rule of linear damage accumulation.

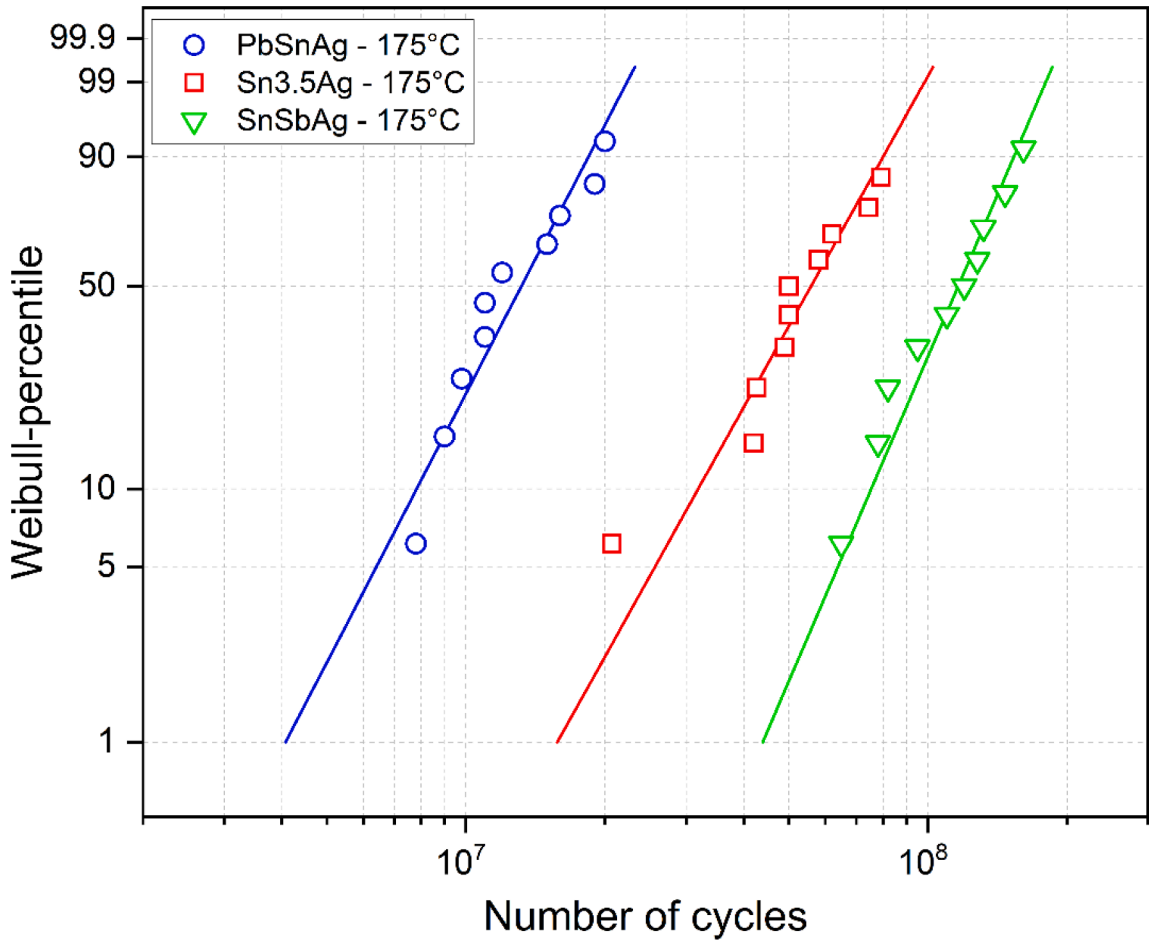

Fig. 6. Weibull plot of samples tested in four point bending with 5.2 μm displacement amplitude at a temperature of 175 °C until lift off from substrate. Lifetimes of the solder alloys PbSnAg (10 samples), Sn3.5Ag (10 samples) and SnSbAg (10 samples) are compared.

Combination of Coffin Manson model with Basquin relation using linear damage accumulation

At the initial stage of the model, the case of zero mean stress is considered where the Goodman relation reduces to the Basquin equation. The Basquin equation (Basquin, 1910) relates the stress amplitude $\Delta\sigma_A$ to the number of loading cycles N_f leading to failure. This relation is described by the power law

$$\Delta\sigma_A = \sigma_f'\left(2N_f\right)^b, \tag{1}$$

where σ_f' and b are material parameters. On the other hand, the lifetime model of Coffin (1971) and Manson and Hirshberg (1964) relates the plastic strain $\Delta\varepsilon_{pl}$ accumulated per loading cycle to the number of loading cycles N_f leading to failure according to the power law

$$\Delta\varepsilon_{pl} = \varepsilon_f'\left(2N_f\right)^d, \tag{2}$$

where ε_f' and d are material parameters. Usually, a combination of the Eqs. (1) and (2) is derived by addition of elastic and plastic strains observed per loading cycle, as first suggested by Morrow (1964). In the present formulation of a lifetime model, however, the damage accumulated per loading cycle is added instead of adding elastic and plastic strains. Consequently, the Basquin relation (1) is here rewritten in terms of a power law for damage accumulation, where the damage D_{el} caused by elastic deformation during a loading cycle evaluates to

$$D_{el} = \alpha\cdot{\Delta\sigma_A}^{\beta}. \tag{3}$$

Here, α and β are material constants. Further, the damage accumulated per loading cycle due to plastic deformation reads as

$$D_{pl} = \gamma\cdot{\Delta\varepsilon_{pl}}^{\delta}, \tag{4}$$

where γ and δ are material constants. Fracture will occur, when the damage

$$D\cdot N_f = D_{el}\cdot N_f + D_{pl}\cdot N_f = \left(\alpha\cdot{\Delta\sigma_A}^{\beta} + \gamma\cdot{\Delta\varepsilon_{pl}}^{\delta}\right)\cdot N_f \tag{5}$$

accumulated in N_f loading cycles reaches a value of 1. Consequently, the number of loading cycles, N_f, leading to failure evaluates to

$$N_f = \left(\alpha\cdot{\Delta\sigma_A}^{\beta} + \gamma\cdot{\Delta\varepsilon_{pl}}^{\delta}\right)^{-1}. \tag{6}$$

Effect of non-zero mean stress

The effect of non-zero mean stress is often calculated according to standard methods of Goodman, Gerber, and Soderberg. Goodman (1899) proposed an equation of the form

$$\frac{\sigma_a}{\sigma_e} + \frac{\sigma_m}{\sigma_u} = 1 \tag{7}$$

where σ_a is the alternating stress, σ_m is the mean stress, σ_u is the ultimate tensile strength and σ_e is the effective alternating stress, which may be inserted for the stress amplitude of Eq. (1).

In the present study, the visco-plastic Anand model is used for solder materials. For this model, the ultimate tensile strength is strain rate dependent. Consequently, we here replace the ultimate tensile strength

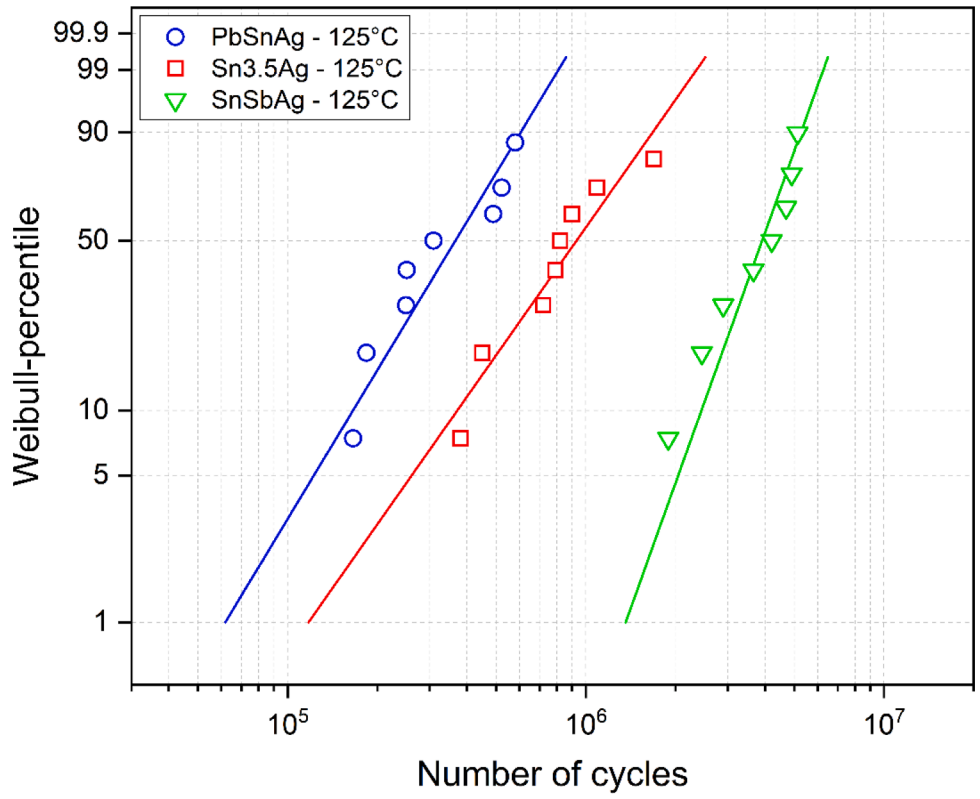

Fig. 7. Weibull plot of samples tested in three point bending with 5.2 μm displacement amplitude at a temperature of 125 °C until lift off from substrate. Lifetimes of the solder alloys PbSnAg (8 samples), Sn3.5Ag (8 samples) and SnSbAg (8 samples) are compared.

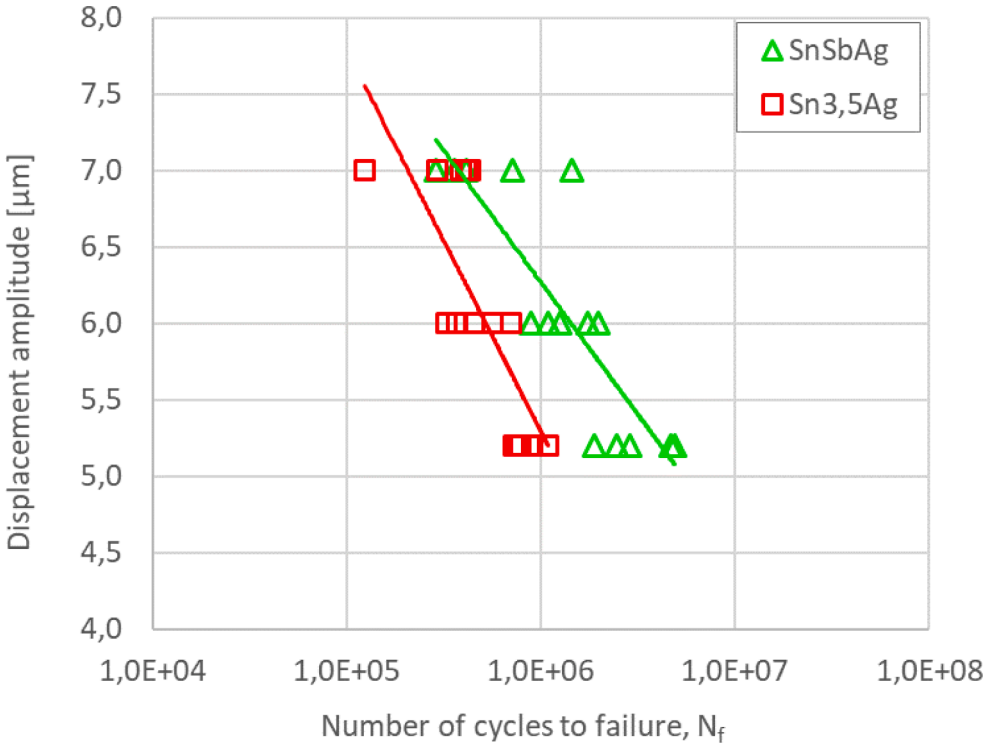

Fig. 8. Number of loading cycles until lift off from substrate versus displacement amplitude. The samples were tested in three-point bending mode at 125 °C. Sn3.5Ag solders are compared to SnSbAg.

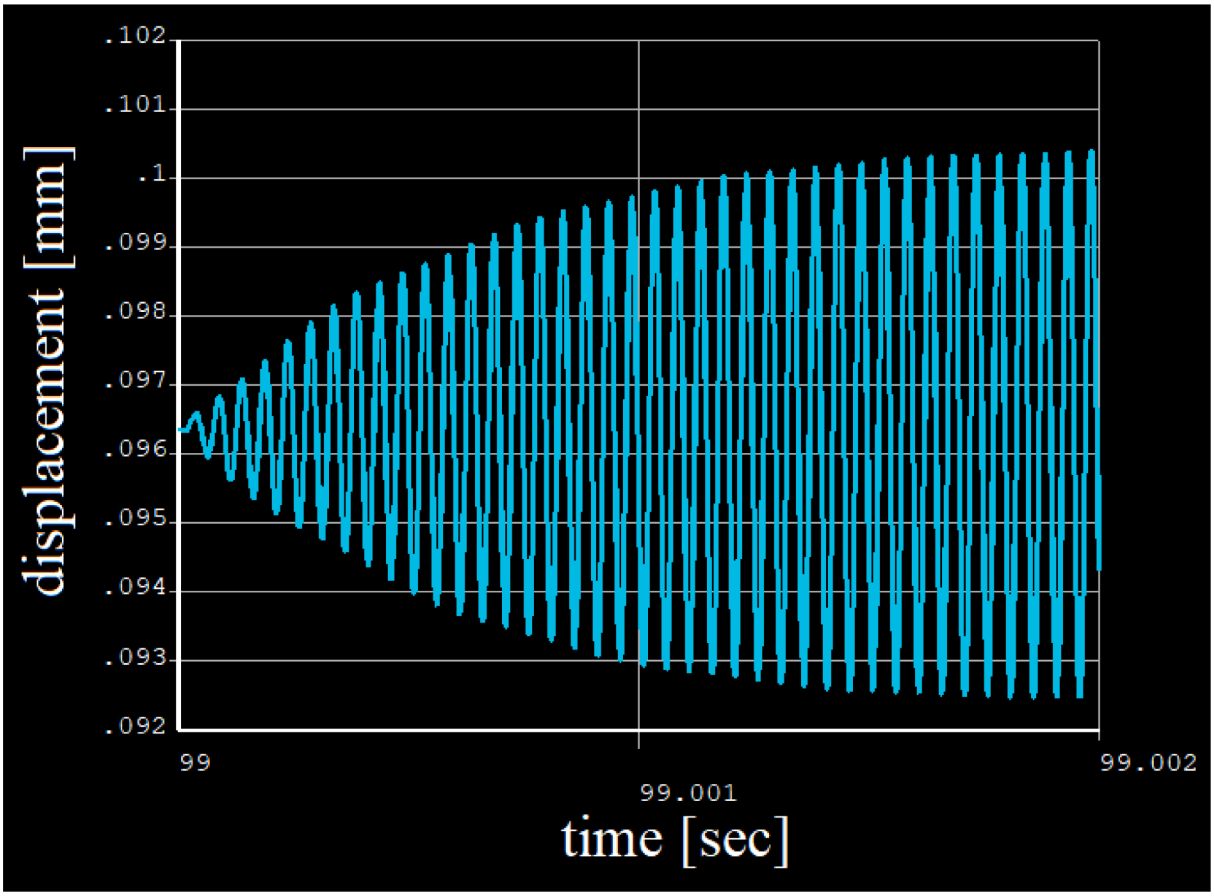

Fig. 9. Plot of nodal displacements versus time for the transient FEM simulation. The first 40 loading cycles of a sample tested in four point bending at 175 °C are shown. The selected node corresponds to the measurement point of the Laser Doppler Vibrometer. The displacement amplitude observed under steady state conditions was 4 μm.

Table 4
Material parameters used in combination with the Anand model.

Parameter	PbSnAg	Sn3.5Ag	SnSbAg
A [sec^{-1}]	1.052 10^5	1.77016 10^5	1.1917 10^4
Q/R [K]	11,028	10,279	7498
s_0 [MPa]	$17.51 - 0.057 \cdot T[^\circ C]$	$18.07 - 0.077 \cdot T[^\circ C]$	$19.85 - 0.082 \cdot T[^\circ C]$
ξ[·]	7	7	3.552
m[·]	0.241	0.207	0.192
h_0 [MPa]	1432	27,782	30,893
$\hat{s}$ [MPa]	41.63	52.4	29.102
n [ ]	0.002	0.0177	0.096
a [ ]	1.3	1.6	1.203

Table 5
Young's modulus E, Poisson ratio ν, coefficient of thermal expansion CTE and density used in the transient FEM simulation. For all materials a stress-free reference temperature of T = 50 °C was assumed in combination with simulation of thermal expansion.

Material	E [GPa]	ν []	CTE [ppm/ °C]	$Density$ [g/cm^3]
PbSnAg	$26.83 - 0.073 \cdot T[^\circ C]$	0.35	29	11.0
Sn3.5Ag	$49.02 - 0.16 \cdot T[^\circ C]$	0.35	22	7.5
SnSbAg	$56.46 - 0.18 \cdot T[^\circ C]$	0.35	31	7.3
Cu	120	0.343	17	8.92
Al_2O_3	350	0.3	7.2	3.69
Si	160	0.27	2.6	2.33

by the strain rate dependent saturation stress σ_{sat}. Further, the saturation stress is here evaluated according to a procedure suggested by Thoben (2002):

The strain rate of the Anand model (Anand, 1985) writes as

$$\dot{\varepsilon} = A \cdot exp\left\{-\frac{Q}{RT}\right\} \cdot \left[sinh\left(\xi \frac{\sigma}{s}\right)\right]^{\frac{1}{m}} \tag{8}$$

where A is the pre-exponential factor, Q is the activation energy, R is the gas constant and T is the absolute temperature in [K]. Further, ξ is called a multiplier of stress, σ is the von Mises stress, s is the deformation resistance and m is the strain rate sensitivity of stress. In this model, the saturation value s^* of the deformation resistance s is

$$s^* = \hat{s} \cdot \left[\frac{\dot{\varepsilon}}{A} exp\left\{\frac{Q}{RT}\right\}\right]^n \tag{9}$$

where $\hat{s}$ is the saturation value of the deformation resistance coefficient, while n is the strain rate sensitivity of s^*. When saturation is reached, the strain rate $\dot{\varepsilon}$ is constant and the deformation resistance s takes the saturation value s^*. Hence, the strain rate dependent value of saturation stress σ_{sat} may be derived from Eq. (8). Following Thoben (2002), one obtains

$$\sigma_{sat}(\dot{\varepsilon}) = \frac{\hat{s}}{\xi} arsinh\left(\left\{\frac{\dot{\varepsilon}}{A} exp\left\{\frac{Q}{RT}\right\}\right\}^m\right) \cdot \left[\frac{\dot{\varepsilon}}{A} exp\left\{\frac{Q}{RT}\right\}\right]^n \tag{10}$$

Now, a multi-axial treatment of the Goodman relation is elaborated, where the effective stress amplitude depends on the evolution of deviatoric stress. At first it is necessary to eliminate the influence of rigid body rotation from the constitutive equations of the model. This is

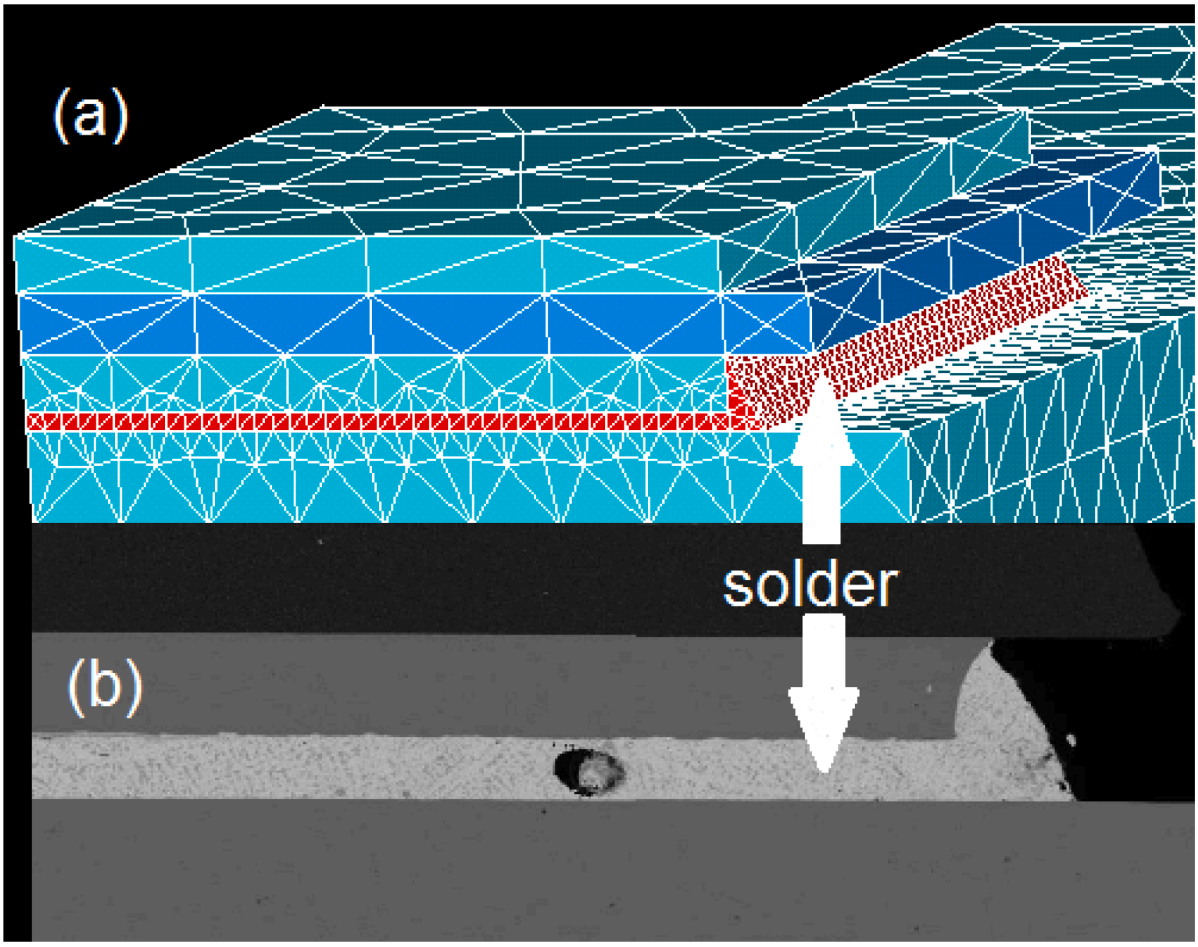

Fig. 10. Detail of the FEM model (a) showing the mesh in the vicinity of the solder interconnect in comparison to the SEM micrograph (b) of the sample.

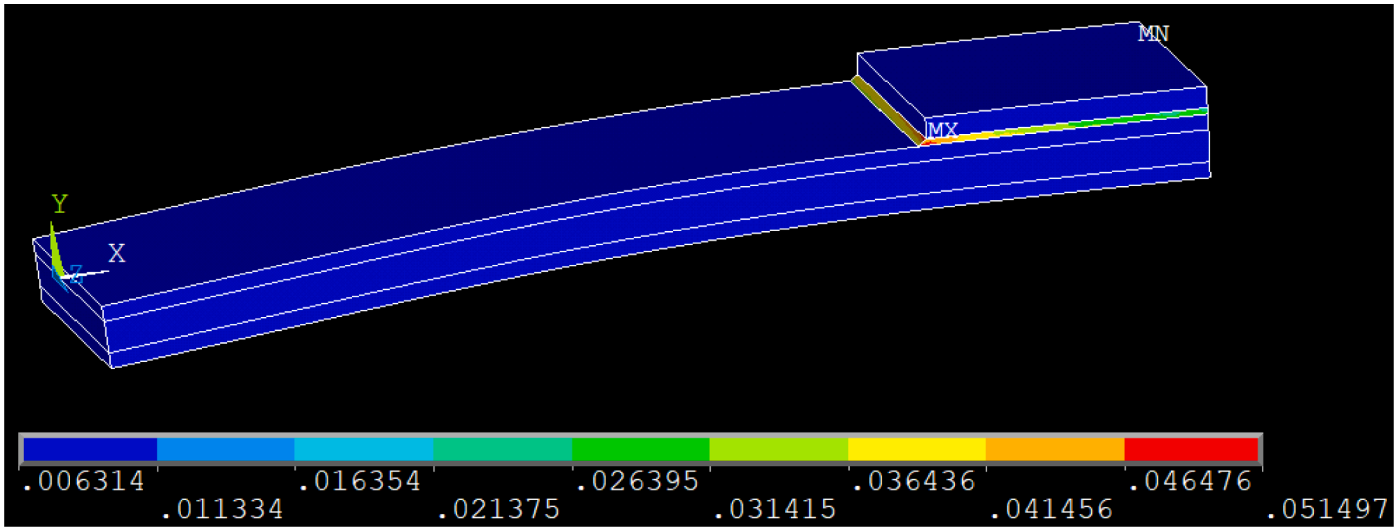

Fig. 11. Plot of accumulated plastic strain in a sample after preloading and 40 consecutive loading cycles tested in four point bending. The ambient temperature was 175 °C and the displacement amplitude was 4 μm. A quarter model was simulated, where the plane $z = 0$ serves as a symmetry plane.

achieved with use of the second Piola-Kirchhoff stress tensor S. Next, the mean values S_{ij}^{mean} of the components S_{ij} of the second Piola-Kirchhoff stress tensor are defined as the time average

$$S_{ij}^{mean} = \frac{1}{\tau}\int_0^{\tau} S_{ij}(t)dt \tag{11}$$

over one period τ. The tensor formed by the components S_{ij}^{mean} is called

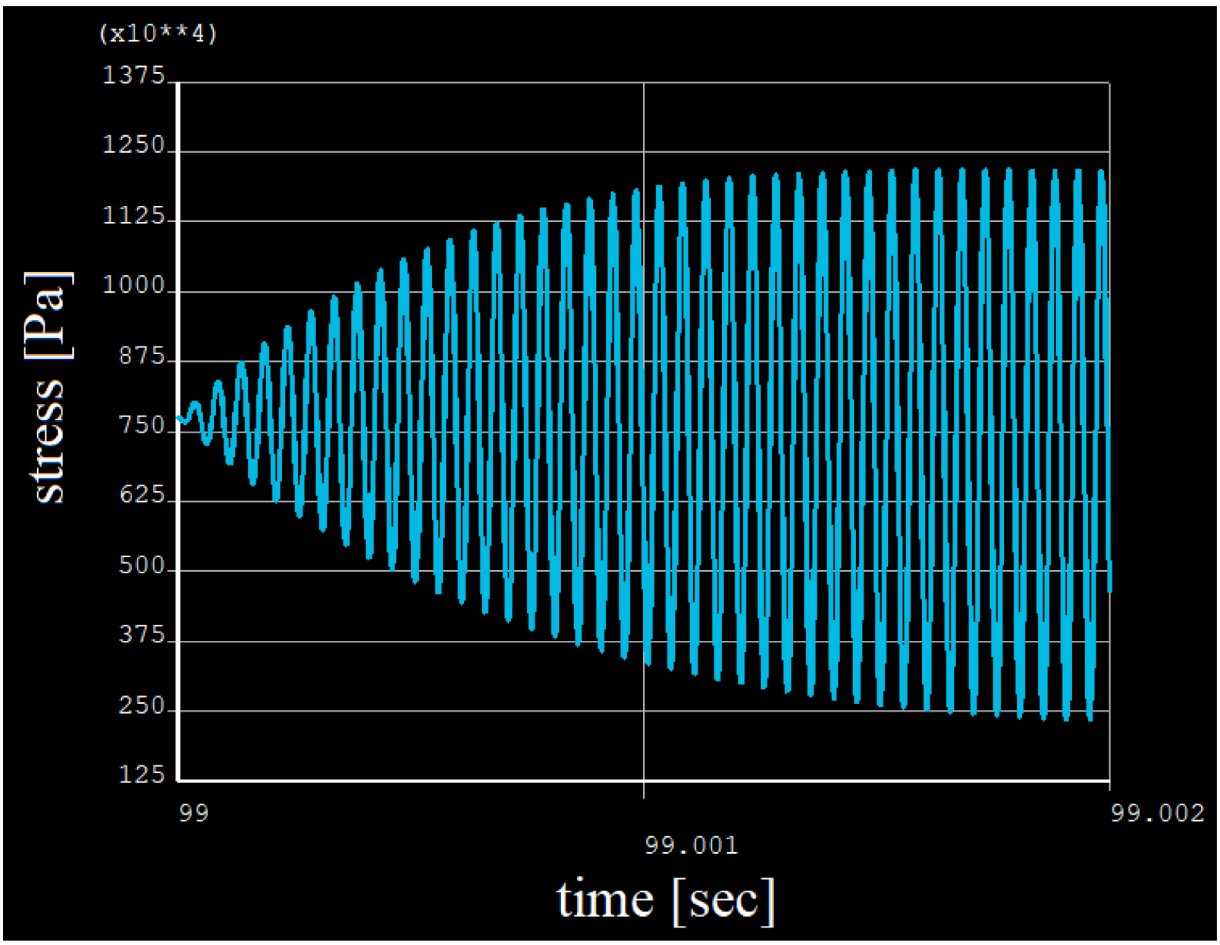

Fig. 12. Evolution of the stress component σ_{11} [Pa] at the critical site of the PbSnAg solder during 40 cycles of periodic loading.

S^{mean}. Further, maximum values S_{ij}^{max} and minimum values S_{ij}^{min} of the tensor components are defined for the period τ, respectively. Thus, the components of the stress amplitude tensor are defined as

$$S_{ij}^{amp} = \frac{1}{2}\left(S_{ij}^{max} - S_{ij}^{min}\right) \tag{12}$$

Next, the influence of deviatoric stress on the fatigue behavior is considered in further detail. It is postulated that the effect of multiaxial deviatoric stress on material fatigue may be evaluated by similarity to the flow rule of J_2 plasticity, thereby following the maximum distortion criterion. Consequently, scalar valued equivalent stresses will be defined for the tensors of mean stress S^{mean} and stress amplitude S^{amp} by analogy to von Mises stress. Thus, the invariant J_2 (Ottosen & Ristinmaa, 2005) of mean stress

$$J_2(S^{mean}) = \frac{1}{2} S_{mean\ ij}^{dev} \cdot S_{mean\ ji}^{dev} \tag{13}$$

is defined, where summation is carried out over repeated indices, and the deviatoric part of the mean stress tensor S^{mean} reads as

$$S_{mean}^{dev} = S^{mean} - \frac{1}{3} tr(S^{mean}) \cdot I. \tag{14}$$

Here, *tr* denotes the trace of a tensor and I is the identity matrix. By analogy to the normalization of von Mises stress, an equivalent mean stress

$$s_{eqv}^{mean} = \sqrt{3 \cdot J_2(S^{mean})} \tag{15}$$

is defined. Further, we define the invariant J_2 of the stress amplitude tensor as

$$J_2(S^{amp}) = \frac{1}{2} S_{amp\ ij}^{dev} \cdot S_{amp\ ji}^{dev} \tag{16}$$

where summation is again carried out over repeated indices, and

$$S_{amp}^{dev} = S^{amp} - \frac{1}{3} tr(S^{amp}) \cdot I \tag{17}$$

is the deviatoric part of S^{amp}. Thus, the equivalent stress amplitude is defined as

$$s_{eqv}^{amp} = \sqrt{3 \cdot J_2(S^{amp})}. \tag{18}$$

Consequently, the constitutive equation of the lifetime model is now written in the form

$$\frac{s_{eqv}^{amp}}{s_{eff}} + \frac{s_{eqv}^{mean}}{\sigma_{sat}} = 1, \tag{19}$$

where s_{eff} is called the effective stress equivalent. Resolving Eq. (19) with respect to s_{eff} yields

$$s_{eff} = \frac{s_{eqv}^{amp} \cdot \sigma_{sat}}{\sigma_{sat} - s_{eqv}^{mean}}, \tag{20}$$

where the saturation stress σ_{sat} is always larger than s_{eqv}^{mean}. The deviatoric stress equivalent s_{eff} can be inserted for $\Delta\sigma_A$ into Eq. (6).

Consequently, one obtains a lifetime model considering two different failure mechanisms, where the first mechanism of damage accumulation is related to the plastic strain, while the second mechanism is related to

alternating stress and mean stress. With the help of Miner's rule, this fatigue model can easily be extended to variable stress levels, where the damage accumulated per cycle is added until the critical value of $D = 1$ is finally reached.

At this point it should be mentioned that damage accumulation during heating and preloading of the samples was also taken into account, but it was found that the reduction of fatigue life due to preloading was only marginal in experiments of the present study.

Influence of temperature on fatigue life

A significant influence of temperature on the parameter α of Eq. (6) was found. To some extent, this temperature dependence can be described by

$$\alpha(T) = \frac{\alpha_0}{E(T)} \tag{21}$$

where *E(T)* is the temperature dependent Young's modulus of the solder material. Thus, the constitutive equation of the temperature dependent lifetime model under isothermal steady state conditions takes the form

$$N_f(T) = \left(\frac{\alpha_0}{E(T)} \cdot {s_{eff}}^{\beta} + \gamma \cdot {\Delta\varepsilon_{pl}}^{\delta}\right)^{-1} \tag{22}$$

where α_0, β, γ and δ are material parameters. Alternatively, the lifetime may be expressed by the equation

$$N_f = \left(\alpha_0 \cdot {\varepsilon_{eff}}^{\beta} + \gamma \cdot {\Delta\varepsilon_{pl}}^{\delta}\right)^{-1} \tag{23}$$

where

$$\varepsilon_{eff} = \frac{s_{eff}}{E} \tag{24}$$

is here called the effective strain equivalent, which is per definition related to the effective stress s_{eff}.

Note that the second Piola-Kirchhoff stress has been used in the afore mentioned equations in order to avoid a contribution to alternating stress arising from pure rotation of a stressed sample. Nevertheless, to a good approximation small deformation theory may be applied if strains and rotations are small enough.

A detailed comparison with experimental data suggests that the parameters α_0, β, γ and δ are in fact temperature dependent. In comparison to room temperature, the fatigue life at elevated temperature appears to be reduced. In the temperature range between room temperature and 175 °C, the values of material parameters may be interpolated linearly:

$$\alpha_0(T) = a_0 + a_1(T - T_R) \tag{25 a}$$

$$\beta(T) = b_0 + b_1(T - T_R) \tag{25 b}$$

$$\gamma(T) = c_0 + c_1(T - T_R) \tag{25 c}$$

$$\delta(T) = d_0 + d_1(T - T_R) \tag{25 d}$$

where $T_R = 25$ °C is here used as reference temperature.

4.4. Results of the lifetime model

The lifetime parameters of equations (25 a-d) are now fitted to experimental data. In a first step, the statistical scattering of lifetime results was eliminated by averaging over results derived for equivalent load levels. The representative experimental lifetimes, which are hereafter used, were summarized in Tables 1-3. In a second step, optimized values for the lifetime parameters were determined using the least square method based on relative error. This procedure involved the extraction of FEM simulation data for accumulated plastic strain and s_{eff} at the critical sample site, where fracture is expected. Thereby, the critical sample site is defined as the point, where the damage variable D defined in Eq. (5) takes a maximum. This location is usually found at a nodal point at the periphery of the solder joint, where the plastic equivalent strain takes its maximum during the last time step of the transient FEM simulation. The position of this maximum is indicated in Figs. 11 and 13 for samples tested in three - and four-point bending, respectively. The values for the parameters of the lifetime model, which

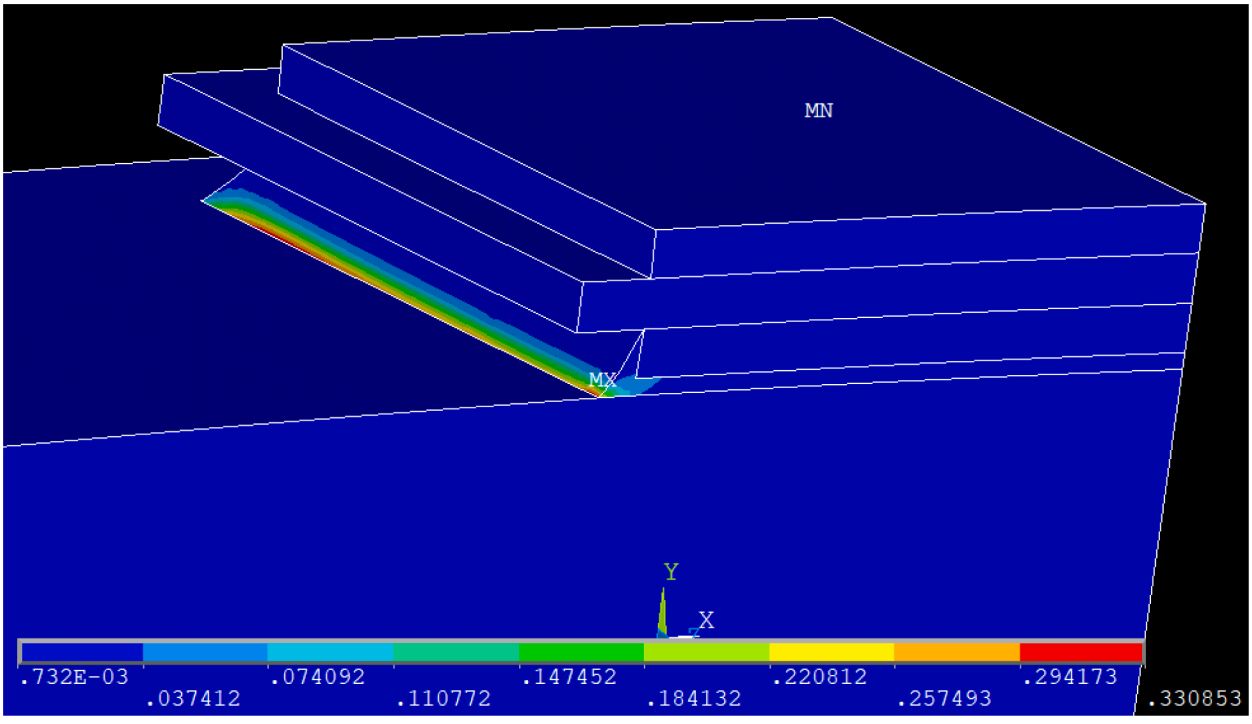

Fig. 13. Plot of accumulated plastic strain after preloading and 24 cycles of periodical load. A sample soldered with Sn3.5Ag tested at 125 °C with 7 μm displacement amplitude is shown. The symbol MX indicates the location of the maximum of accumulated plastic strain. This is the critical site, where first cracking is expected.

Table 6
Optimized parameters of the lifetime model for PbSnAg, Sn3.5Ag and SnSbAg.

Parameter	PbSnAg	Sn3.5Ag	SnSbAg
a_0	12.1	10.4	9.8
a_1	− 0.08	− 0.066	− 0.064
b_0	3.11	2.65	3.13
b_1	− 0.003467	− 0.0006	− 0.004067
c_0	5.6	8.7	8.2
c_1	− 0.03695	− 0.05733	− 0.05387
d_0	4.2	3.5	4.2
d_1	− 0.02	− 0.01533	− 0.02

gave the best fit are summarized in Table 6. A comparison between experimental and theoretical lifetimes in dependence of damage accumulated per loading cycle is shown in Figs. 14–16.

In double logarithmic scale, the theoretical curve of damage variable versus number of cycles to crack initiation reduces to a straight line, as can be seen in Figs. 14–16. It should be noticed that due to the use of averaged lifetime results, the scattering of fatigue results was very small.

Discussion

It has been the aim of the present study to develop a lifetime model which predicts solder fatigue of power electronic devices under service conditions on the basis of accelerated mechanical testing. Thereby, the strain rate and temperature dependence of inelastic deformation was well described by the visco-plastic Anand model. Furthermore, it was here assumed that damage accumulation is closely related to the amount of accumulated plastic strain, and hence the lifetime parameters calibrated at very high strain rates are equally valid at slow deformation rates. However, there are still open questions, and the comparison between accelerated testing methods and fatigue under service conditions will be a challenge of further investigations.

The deformations used in the present test method are bending deformations, while thermomechanical loads may lead to different multiaxial stress conditions. Nevertheless, the fatigue criterion used here is built on a multiaxial stress criterion, which is combined with a criterion related to the amount of accumulated plastic strain. The criterion utilizes the J_2 invariant, which is widely used in plasticity theory. Moreover, the Goodman relation was included in the calculations to account for mean stress effects. Hence, one may expect that the model will in good approximation apply to any kind of multiaxial loading conditions.

The comparison between mechanical tests and thermomechanical loading is provided by Finite Element Analysis. In this context, it should be mentioned that FEM simulation results are sometimes mesh size dependent, in particular when stress concentrations are investigated. Following the weakest link approach, the critical site, where fracture occurs, is usually found at a stress concentration. However, the influence of mesh size dependence can be reduced, when equivalent element sizes are used for comparison of accelerated mechanical tests with thermomechanical loading under service conditions.

In this investigation, it was found that the fatigue life of solder joints is reduced at elevated temperature. Samples exposed to deformations at an ambient temperature of 175 °C fail at comparatively low level of accumulated plastic strain. The temperature dependence of the parameters of the lifetime model could be interpolated linearly in the temperature range between 25 °C and 175 °C. However, linear extrapolation to temperatures outside this range is not suggested here, because of possible nonlinearity. If necessary, the lifetime model can be extended to a larger temperature range, when the temperature dependence of parameters is described by a polynomial function, as suggested by Wang et al. (2019).

Summary and conclusions

A lifetime model for solder joints was proposed, which can be applied to accelerated mechanical testing. Optimized model parameters were determined through numerical fitting of bending experiments with solder joints made of the alloys PbSnAg, Sn3.5Ag and SnSbAg. The time to crack initiation under vibration loading could well be explained with

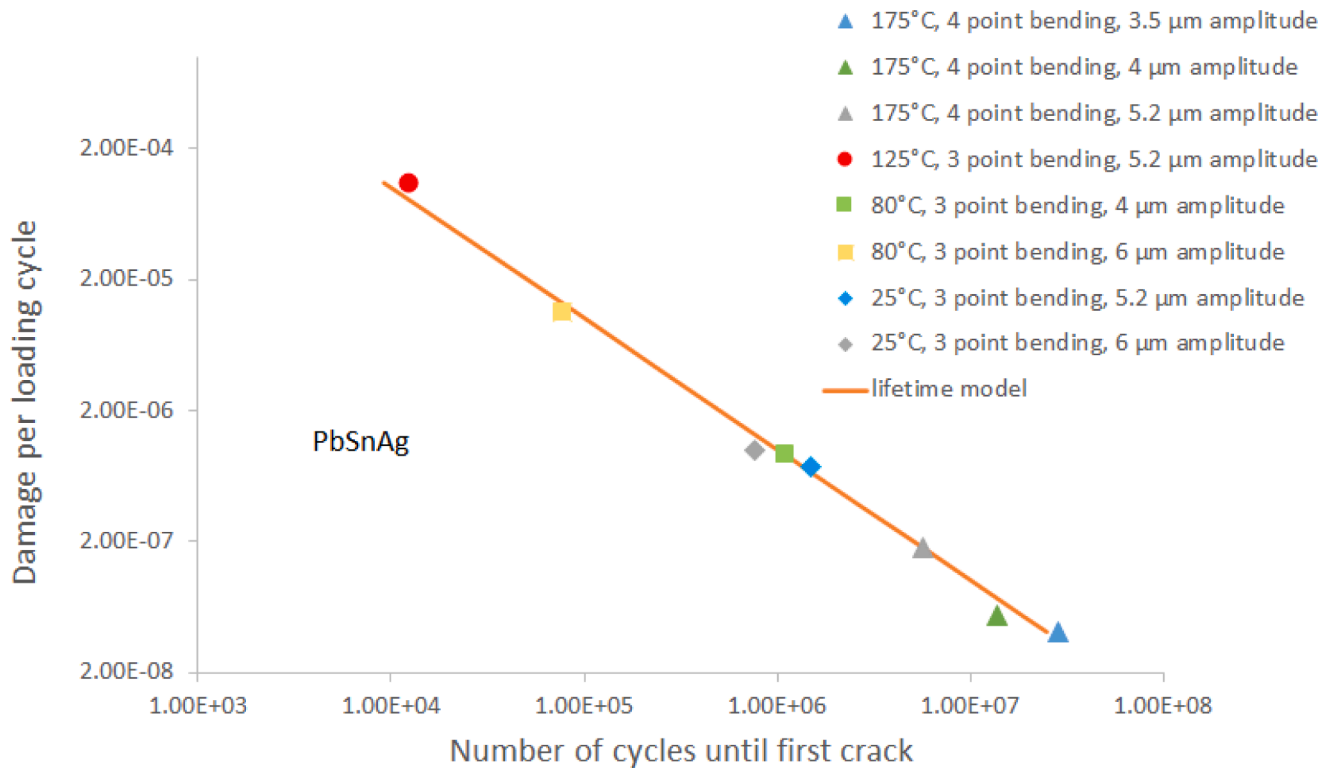

Fig. 14. The lifetimes of the model compared to averaged experimental lifetime data for PbSnAg. A double logarithmic scale plot is shown.

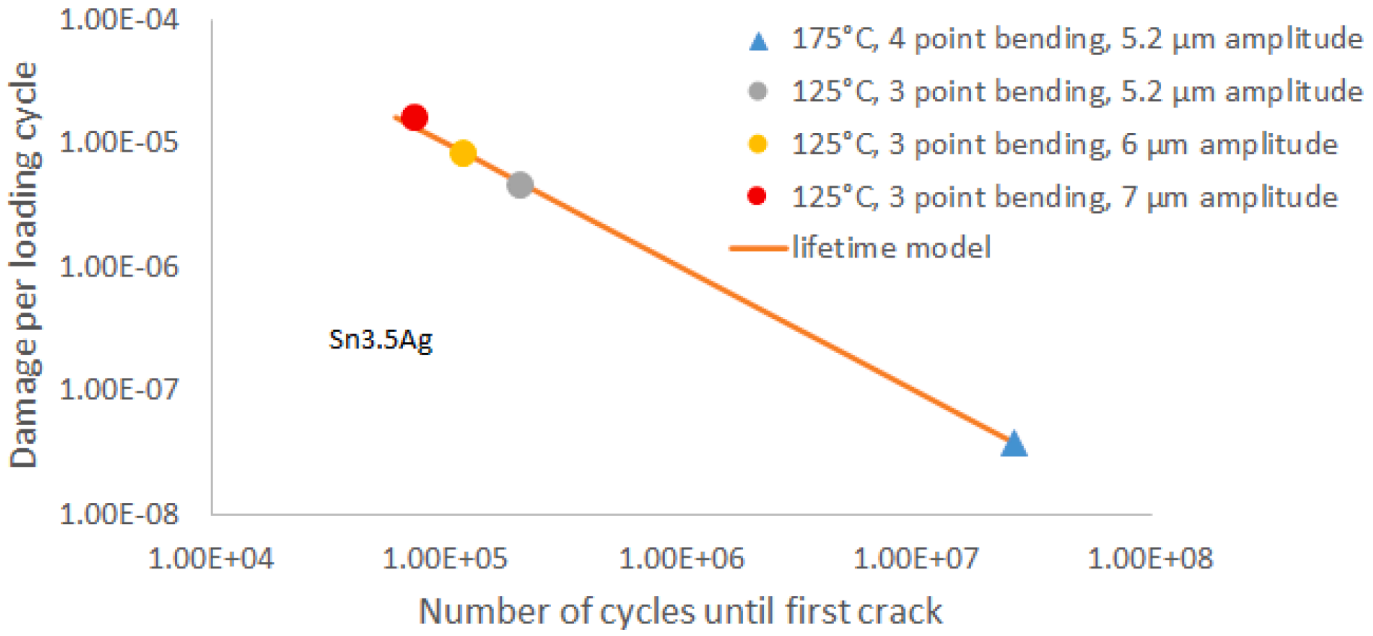

Fig. 15. The lifetimes of the model compared to averaged experimental lifetime data for Sn3.5Ag.

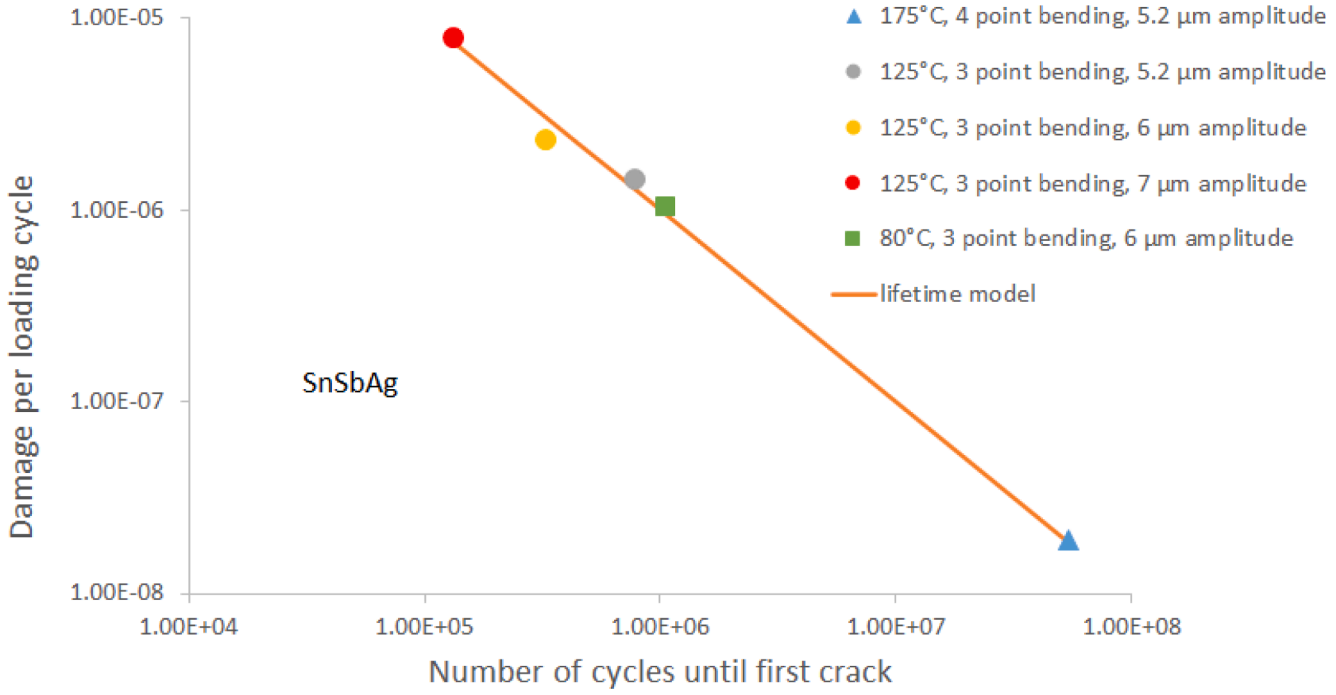

Fig. 16. The lifetimes of the model compared to averaged experimental lifetime data using parameters of Table 6 for SnSbAg.

this approach. The bending experiments at various temperatures were simulated with the Finite Element computer software ANSYS 2020. Fracture initiation occurs at the node, where the damage variable of the lifetime model takes a maximum. The number of loading cycles leading to crack initiation was evaluated on the basis of stresses and strains observed at the critical site of the solder.

The lifetime model is a combination of the Coffin-Manson model with a multiaxial treatment of the Goodman relation. Rigid body rotations, which obviously do not contribute to fatigue, were eliminated by use of the Piola-Kirchhoff stress tensor. Further, the mean stress and the alternating stress, which are inserted into the Goodman relation, were evaluated with the help of the invariant J_2. In conclusion, we obtained a lifetime model, where the four model parameters can be interpolated linearly in the temperature range from 25 °C to 175 °C.

In conclusion, a lifetime model predicting the time to first crack initiation was obtained. Owing to the temperature and strain rate dependence included in the visco-plastic Anand model, one may use the results of accelerated mechanical testing in order to predict thermo-mechanical fatigue under service conditions of power electronic modules. Thereby, the setup of the ultrasonic fatigue experiment reaches the number of loading cycles, which are observed after 10 years of service already after a few hours of testing.

Declaration of Competing Interest

The authors have no affiliation with any organization with a direct or indirect financial interest in the subject matter discussed in the manuscript.

Data availability

Some part of the research data are confidential. Other data will be made available on request.

Acknowledgements

The financial support by the Austrian Federal Ministry for Digital and Economic Affairs and the National Foundation for Research, Technology and Development is gratefully acknowledged

References

Anand, L. (1985). Constitutive equations for hot working of metals. *International Journal of Plasticity, 1*, 213–231.

Basquin, O. H. (1910). The exponential law of endurance tests. *Proceedings-American Society for Testing and Materials, 10*, 625–630.

Chen, X., Chen, G., & Sakane, M. Proceedings of Intersociety Conference Thermal and Thermo-mechanical Phenomena in Electronic Systems Vol. 2 (2004), p. 447.

Cheng, Z. N., Wang, G. Z., Chen, L., Wilde, J., & Becker, K. (2000). „Viscoplastic Anand model for solder alloys and its Application". *Soldering & Surface Mount Technology, 12/2*, 31–36.

Coffin, L. F. (1971). *Journal of Materials, 6*, 388.

Czerny, B., Lederer, M., Nagl, B., Trnka, A., Khatibi, G., & Thoben, M. (2012). Thermo-mechanical analysis of bonding wires in IGBT modules under operating conditions. *Microelectronics Reliability, 52*, 2353–2357.

Dudek, R., Kreyssig, K., Rzepka, S., Novak, M., Gruebl, W., Fruehauf, P., et al. (2019). *Comparisons of solder joints fatigue life predictions and several long term testing results*. IEEE ITHERM Conference.

El-Daly, A. A., Fawzy, A., Mohamad, A. Z., & El-Taher, A. M. (2011). Microstructural evolution and tensile properties of Sn–5Sb solder alloy containing small amount of Ag and Cu. *Journal of Alloys and Compounds, 509*, 4574–4582.

Engelmaier, W. (1983). Fatigue Life of Leadless Chip Carrier Solder Joints During Power Cycling. In *, CHMT 6. IEEE Transactions on components, hybrids, and manufacturing technology*. Sept.

Goodman, J. (1899). *Mechanics applied to engineering*. London: Longman, Green & Company.

Herrmann, T., Feller, M., Lutz, J., Bayerer, R., & Licht, T. (2007). „Power Cycling Induced Failure Mechanisms in Solder Layers". *European Conference on Power Electronics and Applications*.

Kobayashi, T., Kobayashi, K., Mitsui, K., & Shohji, I. (2018). Comparison of Sn-5Sb and Sn-10Sb Alloys in Tensile and Fatigue Properties Using Miniature Size Specimens. *Hindawi Advances in Materials Science and Engineering*. Article ID 1416942.

Libot, J. B., Arnaud, L., Dalverny, O., Alexis, J., Milesi, P., & Dulondel, F. (2016). Mechanical fatigue assessment of SAC305 solder joints under harmonic vibrations. In *Proceedings of ICEP*.

Mainka, K., Thoben, M., & Schilling, O. (2011). *Lifetime calculation for power modules, application and theory of models and counting methods*. Conference: Power Electronics and Applications. EPE.

Manson, S. S., & Hirshberg, M. H. (1964). Fatigue, an Interdisciplinary Approach. In *Proceedings of the X Sagamare Army Materials Research Conference* (p. 133). Syracuse University Press.

Marsh, G., Wignall, C., Thies, Ph. R., Barltrop, N., Incecik, A., Venugopal, V., et al. (2016). Review and application of Rainflow residue processing techniques for accurate fatigue damage estimation. *International Journal of Fatigue, 82*, 757–765.

Miner, M. A. (1945). Cumulative damage in fatigue. *Journal of Applied Mechanics, 12*(3), 159–164.

Morrow, J. (1964). Cyclic Plastic Strain Energy and Fatigue of Metals. *Internal friction, damping, and cyclic plasticity* (pp. 45–87). ASTM Special Technical Publication No.

Murty, K. L., Haggag, F. M., & Mahidhara, R. K. (1997). Tensile, creep and ABl tests on Sn5%Sb solder for mechanical property evaluation. *Journal of Electronic Materials, 26*(7).

Ottosen, N. S., & Ristinmaa, M. (2005). *The mechanics of constitutive modeling*. Elsevier.

Salmela, O., Andersson, K., Perttula, A., Särkkä, J., & Tammenmaa, M. (2008). Modified Engelmaier's model taking account of different stress levels. *Microelectronics Reliability, 48*, 773–780.

Sathik, M., Jet, T.K., Gajanayake, C.J., Simanjorang, R., & Gupta, A.K. Comparison of power cycling and thermal cycling effects on the thermal impendance degradation in IGBT modules, IECON 2015-Yokohama.

Schmidt, R., & Scheuermann, U. (2012). Separating failure modes in power cycling tests, CIPS 2012, March, 6–8. Nuremberg/Germany: IEEE. Paper 04.4.

Susmel, L., Tovo, R., & Lazzarin, P. (2005). The mean stress effect on the high-cycle fatigue strength from a multiaxial fatigue point of view. *International Journal of Fatigue, 27*, 928–943.

Thambi, J., Tetzlaff, U., Schiessl, A., Langc, K.-. D., & Waltz, M. (2016). High cycle fatigue behaviour and generalized fatigue model development of lead-free solder alloy based on local stress approach. *Microelectronics Reliability, 66*, 98–105.

Thoben, M. (2002). Zuverlässigkeit von großflächigen Verbindungen in der Leistungselektronik, Ein Beitrag zum „Design for Reliability" Fortschritt-Berichte VDI, Reihe 9. *Elektronik/Mikro- und Nanotechnik, Nr, 363*.

Wang, X., Zhang, W., Zhang, T., Gong, J., & Wahab, M. A. (2019). A New Empirical Life Prediction Model for 9–12%Cr Steels under Low Cycle Fatigue and Creep Fatigue Interaction Loadings". *Metals, 9*, 183.

Wilde, J., Becker, K., Thoben, M., Blum, W., Jupitz, T., Wang, G., et al. (2000). Rate Dependent Constitutive Relations Based on Anand Model for 92.5Pb5Sn2.5Ag Solder. In *, 23. IEEE transactions on advanced packaging*. August.

Yu, D., Al-Yafawi, A., Nguyen, T. T., Park, S., & Chung, S. (2011). High-cycle fatigue life prediction for Pb-free BGA under random vibration loading. *Microelectronics Reliability, 51*, 649–656.